IEEE Photonics Journal
An IEEE Photonics Society Publication

Open Access

Quantitative Phase Imaging During Cell Division Based on Dual-Channel Microscopic Interferometry System

Volume 12, Number 1, February 2020

Shengde Liu
Dejin Zheng
Jiaosheng Li
Jindong Tian
Liyun Zhong
Xiaoxu Lu

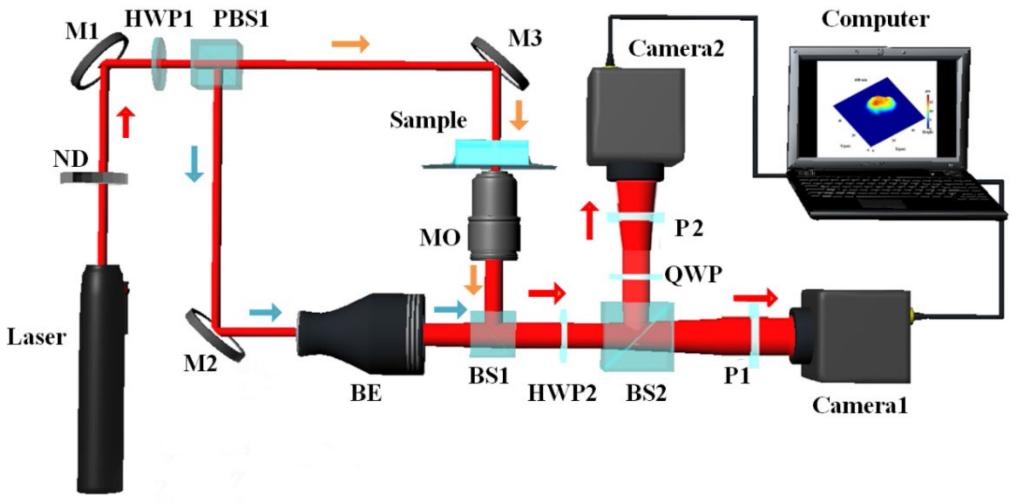

DOI: 10.1109/JPHOT.2019.2955751

IEEE photonics SOCIETY
IEEE

Quantitative Phase Imaging During Cell Division Based on Dual-Channel Microscopic Interferometry System

Shengde Liu,[1] **Dejin Zheng**,[1] **Jiaosheng Li**,[1] **Jindong Tian**,[2] **Liyun Zhong**,[1] **and Xiaoxu Lu** [1]

[1]Guangdong Provincial Key Laboratory of Nanophotonic Functional Materials and Devices, South China Normal University, Guangzhou 510006, China
[2]Shenzhen Key Laboratory of Micro-Nano Measuring and Imaging in Biomedical Optics, College of Optoelectronic Engineering, Shenzhen University, Shenzhen 518060, China

DOI:10.1109/JPHOT.2019.2955751

Manuscript received October 23, 2019; revised November 17, 2019; accepted November 20, 2019. Date of publication December 5, 2019; date of current version January 24, 2020. This work was supported in part by the National Natural Science Foundation of China (NSFC) under Grants 61727814, 61575069 and 61475048. This article has supplementary downloadable material available at http://ieeexplore.ieee.org, provided by the authors. Corresponding author: Xiaoxu Lu (e-mail: hsgd-zlxx@scnu.edu.cn).

Abstract: Quantitative phase imaging (QPI) during cell division is implemented by ourhomemade dual-channel microscopic interferometry (DCMI) system. A pair of interferograms with a fixed phase shift of $\pi/2$ is simultaneously captured by the DCMI system, and two-step phase demodulation algorithm is employed for phase retrieval. By capturing a sequence of paired-interferograms with the DCMI system, we achieve the dynamic QPI during cell division, and then the cellular surface area, volume and the ratio of surface area to volume (RSV) and their variations. Both the reliability and stability of the DCMI system are verified. In addition to maintaining the advantages of optical interferometry, this DCMI system is very suitable for dynamic QPI due to its rapid speed of phase retrieval. Importantly, this DCMI based QPI method will supply a powerful tool for studying the precise mechanism during cell division, differentiation, apoptosis and other dynamic processes.

Index Terms: Quantitative phase imaging, dual-channel microscopic interferometry, phase shift, cell division.

1. Introduction

Along with the development of cell biology, it is urgently-needed to achieve dynamic quantitative phase image (QPI), and calculate cellular surface area, volume, refractive index and dry mass during cell division, differentiation, and apoptosis [1]–[5]. To date, many non-interferometry and interferometry methods are introduced for QPI based on the different requirements, such as high acquisition rate for high temporal resolution in flow imaging and mass profiling [6], [7], in situ monitoring of growing adherent cells [8]–[10], living cell tomography [11], [12]. Since only one-frame image requires to be collected, non-interferometry methods, such as the Shack-Hartmann [13]–[15], Plenoptic sensor [16]–[18], have inherent advantages in dynamic data acquisition. However, the use of micro-lens arrays and the limited number of pixels in sensors greatly restrict the resolution of non-interferometry methods, and the situation would be worse when the small sample is tested. Though someiteration based non-interferometry algorithms, such as Gerchberg–Saxton and its descendent Fienup's phase retrieval algorithms [19], [20], have been widely used, although

their intrinsic mechanism isclear physically, they still difficult to achieve dynamic QPI due to a large amount of calculations. In particular, failure of convergenceand stagnation of the iterates making these algorithms hard to satisfy the dynamic QPI of living cell. Recently, based on the light intensity analysis, the solution of intensity transfer equation (TIE) [21], [22] is introduced, in which the quantitative phase information can be achieved from the transmission field distribution of measured sample, but it is required to satisfy rigorous displacement of measured sample at the focal plane, as well as the additional boundary condition and a large amount of calculations. Therefore, these methods are still difficult to achieve accurate QPI of dynamic process [23]. Optical interferometry, revealing the advantages of high accuracy,non-destructive, high resolution and label-free, is becoming a good candidate for QPI. Unlike the conventional phase contrast microscopy (PC) [24] and differential interference contrast microscopy (DIC) [25] which are only suitable for observing cells by human eyes [26], the intensity of a pixel in the interferometry based QPI has direct physical meaning, making it ideal data for computer processing. Of all the interferometry methods, the off-axis and spatial domain phase-shifting methods, in which the Fourier transform [23] and Hilbert transform [27] are utilized to perform phase retrieval of measured sample, but the corresponding accuracy is affected by the noise and size of filtering window. To improve the accuracy, Mach-Zehnder interferometry [28], Michelson interference microscopy [29], Linnik interferometry [30] are developed, and the reconstruction accuracy of the phase and amplitude images from the recorded interferograms varies with the hardware configuration. Overall,these technologies have achieved some cellular state characterization parameters, such as dry mass [31], activity [32], intracellular homeostasis exploration and cellular apoptosis and traction measurement [33], [34] with relative high accuracy. Specially, due to the advantage of high accuracy, the dynamic QPI methods based on phase-shifting interferometry are developed, in which the role issue is to capture several interferograms with different phase shifts by using different methods, such as using different region of CCD or CMOS target [35], [36], or using the polarized phase-shifting array template to create a photoelectric conversion array on the four pixels as a unit and then form a pixel phase shifting camera with the phase shifts of $\pi/2$ [37], or splitting multiple sub-interferograms with a certain phase shifts from one-frame interferogram with additional spatial carrier [38]–[40]. In all above methods, though the simultaneous spatial phase-shifting interferometry can be utilized to achieve dynamic QPI, the measuring accuracy is still not very highdue to lowering down the resolution of the system [35], [36], or the very complicated fabrication of the polarized phase-shifting array and errors due to the pixel mismatching [37], or the introduction of spatial carrier whose spatial frequency limits the spatial frequency of the sample [38]–[40].

In this study, we implement the QPI during cell divisionby using a homemade dual-channel microscopic interferometry (DCMI) system, in which a pair of interferograms with afixed phase-shift of $\pi/2$ is simultaneously captured and the phase of cell sample is calculated by two-step phase demodulation algorithm. Using the proposed DCMI system, we achieve the dynamic QPI during cell division.

2. Principle

2.1 Structure of Dual-channel Microscopic Interferometry System

Figure 1 shows the architecture of dual-channel microscopic interferometry (DCMI) system, in which the micro-imaging subsystem consists of a sample stage, micro-objective and camera, and the system lateral resolution depends on the numerical aperture of micro-objective. To solve the spatial mismatch, the cameras were calibrated in five dimensions (x, y, z, pitch, yaw) before capturing interferograms.

For ease of understanding, we choose the Jones matrix to explain the principle of QPI by the above DCMI system: Assuming $\left[\begin{smallmatrix}\cos(2\alpha) & \sin(2\alpha)\\ \sin(2\alpha) & -\cos(2\alpha)\end{smallmatrix}\right]$ denotes the half-wave plate Jones matrix with an angle α between the fast axis and horizontal direction, and $\left[\begin{smallmatrix}\cos^2\beta+i\sin^2\beta & \sin\beta\cos\beta(1-i)\\ \sin\beta\cos\beta(1-i) & \sin^2\beta+i\cos^2\beta\end{smallmatrix}\right]$ is the quarter-wave plate withan angle β between the fast axis ofand horizontal direction.

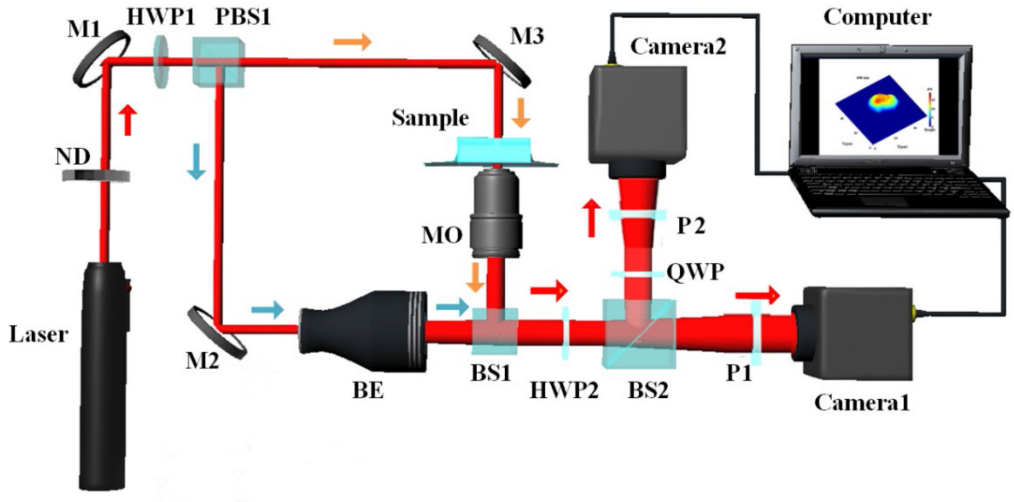

Fig. 1. Sketch of dual-channel microscopic interferometry (DCMI) system. ND: neutral density filter; M1, M2, M3: mirror; HWP1, HWP2: half-wave plates; QWP: quarter-wave plate; BS1, BS2: beam splitters; PBS1, PBS2, PBS3: polarized beam splitters; BE: beam expander; MO: micro-objective.

If a linear polarization laserwith an angle θ between polarization direction and horizontal direction, the corresponding Jones matrixcan be expressed as

$$\begin{bmatrix} \cos\theta \\ \sin\theta \end{bmatrix} \tag{1}$$

Whenthe laser passesthrough HWP1, polarized beam splitter (PBS1), the corresponding Jones matrix can be writtenby

$$\begin{bmatrix} 0 & 0 \\ 0 & 1 \end{bmatrix} \begin{bmatrix} \cos(2\alpha_1) & \sin(2\alpha_1) \\ \sin(2\alpha_1) & -\cos(2\alpha_1) \end{bmatrix} \begin{bmatrix} \cos\theta \\ \sin\theta \end{bmatrix} = \begin{bmatrix} 0 \\ \sin(2\alpha_1 - \theta) \end{bmatrix} \tag{2}$$

Here, PBS1 serves for two purposes: one is to produce two linear polarized light beams with orthogonal polarization directions; the other one is to adjust the intensity ratio of reference beam and object beam by combining HWP1. Thus, the object beam modulated by the sample can be expressed as

$$\begin{bmatrix} 0 \\ A_o \sin(2\alpha_1 - \theta + \varphi_o) \end{bmatrix} \tag{3}$$

where A_o denotes the amplitude modulation function, φ_o is the modulated phase.

The linear polarization laser reflected by PBS1 (the reference beam) can be writtenas

$$\begin{bmatrix} 1 & 0 \\ 0 & 0 \end{bmatrix} \begin{bmatrix} \cos(2\alpha_1) & \sin(2\alpha_1) \\ \sin(2\alpha_1) & -\cos(2\alpha_1) \end{bmatrix} \begin{bmatrix} \cos\theta \\ \sin\theta \end{bmatrix} = \begin{bmatrix} \cos(2\alpha_1 - \theta) \\ 0 \end{bmatrix} \tag{4}$$

After the superposition of object beam and reference beam on a 5:5 beam splitter(BS1) and passing through the HWP2

$$\begin{bmatrix} \cos(2\alpha_2) & \sin(2\alpha_2) \\ \sin(2\alpha_2) & -\cos(2\alpha_2) \end{bmatrix} \begin{bmatrix} \cos(2\alpha_1 - \theta) \\ A_o \sin(2\alpha_1 - \theta + \varphi_o) \end{bmatrix}$$

$$= \begin{bmatrix} \cos(2\alpha_2)\cos(2\alpha_1 - \theta) + \sin(2\alpha_2) A_o \sin(2\alpha_1 - \theta + \varphi_o) \\ \sin(2\alpha_2)\cos(2\alpha_1 - \theta) - \cos(2\alpha_2) A_o \sin(2\alpha_1 - \theta + \varphi_o) \end{bmatrix} \tag{5}$$

After the filtering by the vertical polarizer P1, the incident light on the CCD1 can be expressed as

$$\sin(2\alpha_2)\cos(2\alpha_1-\theta)-\cos(2\alpha_2)A_o\sin(2\alpha_1-\theta+\varphi_o) \tag{6}$$

After the phase shiftsimplemented by QWP and the filtering achieved by the horizontal polarizer P2, the incident beam on the CCD2can be writtenas

$$\begin{aligned}&(\cos^2\beta+i\sin^2\beta)\cos(2\alpha_2)\cos(2\alpha_1-\theta)+\sin\beta\cos\beta(1-i)\sin(2\alpha_2)\cos(2\alpha_1-\theta)\\&+[(\cos^2\beta+i\sin^2\beta)\sin(2\alpha_2)-\sin\beta\cos\beta(1-i)\cos(2\alpha_2)]A_o\sin(2\alpha_1-\theta+\varphi_o)\end{aligned} \tag{7}$$

InEqs. (6) and (7), by setting the parameters $\theta=0;\ \alpha_1=\pi/4;\ \alpha_2=\pi/8;\ \beta=\pi/4$, we can achieve a pair of incident beams with the phase shift of $\pi/2$, whichcan respectively be expressed as

$$\frac{\sqrt{2}}{2}A_o\cos\varphi_o \tag{8}$$

$$i\frac{\sqrt{2}}{2}A_o\cos\varphi_o \tag{9}$$

As the above analysis, the beams of two channels always maintains a fixed phase shift of $\pi/2$ which is only determined by a set of angle parameters, this make it different from conventional interferometry whose phase shift is generated in air retardation and is sensitive to vibration and air turbulence, better resistanceperformance of the DCMI system on the vibration and other external noise pave the way for long lasting stability and accuracy of QPI.

2.2 Phase Retrieval

The intensity distributions of a pair of interferograms with the phase-shift of $\pi/2$ captured by two cameras can be written as

$$I_1(x,y,t)=A(x,y)+B(x,y)\cos[\varphi_o(x,y,t)] \tag{10}$$

$$I_2(x,y,t)=A(x,y)+B(x,y)\cos[\varphi_o(x,y,t)+\pi/2] \tag{11}$$

Here, $A(x,y)$ and $B(x,y)$ represents the background and modulation depth respectively. In general, $A(x,y)$ can be considered as anunchanged parameter. In order to remove thebackground $A(x,y)$, a pair of interferograms of culture dish and medium without cell sample are captured to calculatethe background phase (Figs. 2(a) and (b)). Then, another pair of interferograms of culture dish and medium with cell sample are captured (Figs. 2(c) and (d)). After performing the subtraction operation from equation (10) and (11), the measuredphase can be expressed as

$$\varphi(x,y,t)=-\arctan[I_2(x,y,t)/I_1(x,y,t)] \tag{12}$$

Where, the modulation depth $B(x,y)$, which was determined by the ratio of object beam and reference beam and is usually inconsistent, was normalized in equation (12) thus improving the signal to noise ratio and contrast of the whole frame. It should be noticed that usually the 2D phase unwrapping should be carried out before phase retrieval due to the phase ambiguity in both space and time domain.In the case of our DCMI system and cell measurement, the high resolution in space and time domain from the objective lens and high frame rate, satisfies the condition of Itoh's phase unwrapping algorithm [41] where no phase jump of more than one wavelength occurs between the two pixelsor two frames. Thus, the phase unwrapping can be obtained by performing linear integration of the phase gradient.

Finally, the relationship between the phase and height of the measured sample can be expressed as

$$h(x,y,t)=\frac{\lambda\varphi(x,y,t)}{2\pi(n-n_0)} \tag{13}$$

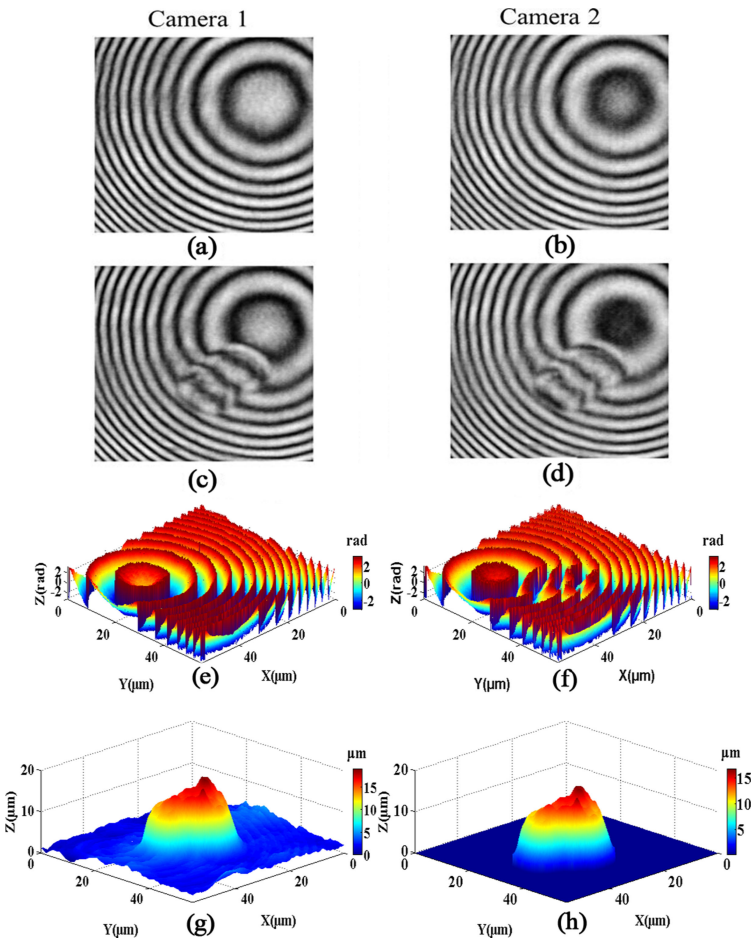

Fig. 2. Experimental result of a living cell with the proposed DCMI system, a pair of interferograms of culture dish and medium (a) (b) without cell; (c) (d) with cell; (e) (f) the wrapped phase distributions without and with cell, respectively; 3D topographic distributions of a living cell implemented by (g) (h) without and with the edge extraction, respectively; in which the size of interferograms is 400 × 400 pixels.

where n denotesthe refractive index of cellular dry mass which is directly related to the measured phase and is a good indicator for cell growth; n_0 represents the refractive index of culture medium, and λ is the laser wavelength.

Subsequently, the surface area of a living cellcan bedetermined by

$$S(t) = \sum_{N(t)} \frac{L(x, y, t)\Delta l}{M} \tag{14}$$

Then, the volume of a living cell can be calculated by

$$V(t) = \sum_{N(t)} \frac{h(x, y, t)\Delta S}{M^2} \tag{15}$$

where $L(x, y, t)$ represents the length of cell profile curve of one pixel, Δl denotes the size of one pixel;ΔS represents the surface area of one pixel; M represents the lateral magnification of DCMI system; $N(t)$ represents the total pixels number of cell at the moment of t.

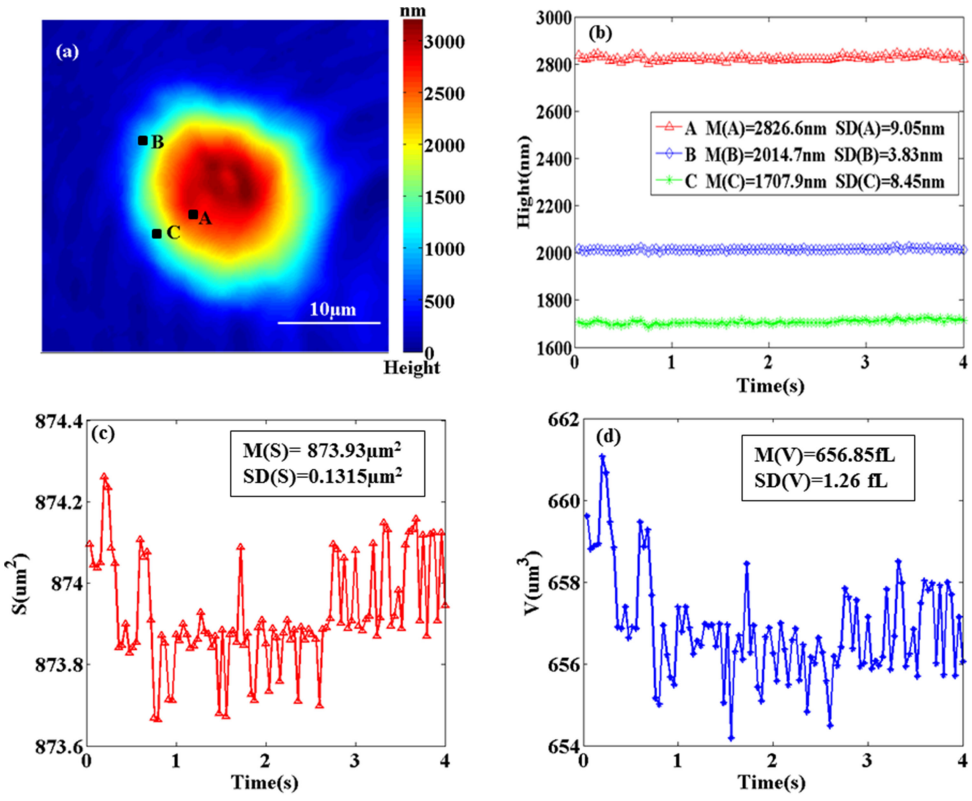

Fig. 3. (a) Topographic distribution of a living CT-26 cell; for a long measuring time; (b) the height variations of three points A, B, C marked in (a) with the average heights of A(M(A)), B(M(B)), C(M(C)) and the standard deviations of SD(A), SD(B), SD(C), respectively; (c) the variation of surface area with the mean surface of M(S) and the standard deviation of SD(S); (d) the volume variation with the mean volume of M(V)) and the standard deviation of SD(V)), in which 1 fL denotes 1 μm^3.

2.3 Stability Testing

Experiment are employed to verify the stability of DCMI system. First, a frequency stabilized He-Ne laser with wavelength of 632.8 nm and micro-objective with NA of 0.4 and magnification of 25 are employed. In our experiment, the magnification of DCMI system is set as 72. Two same cameras (MTV-1802CB) with pixel size of 10 μm $\times$ 10 μm are utilized to capture a pair of interferograms with the phase shift of $\pi/2$ using the speed of 25-frame/second. Immobilized mouse colon cancer cell (CT-26) is chosen as the measured sample. Experiment is carried out on a vibration-isolated platform, and 100-pair interferograms are captured, and the cellular phase and topographic information are calculated according to the above method, as shown in Fig. 3(a). And from Figs. 3(b), it is found that for a long measuring time, the single point result of repeated measurement reveals the low standard deviation, indicating the good stability of proposed DCMI system. Moreover, Figs. 3(b) and 3(d) shows that the low standard deviations for both cellular surface area and volume, further revealing the good stability and high accuracy of proposed DCMI method.

3. QPI During Cell Division

Following, by capturing a sequence of paired interferograms during cell division, we will perform dynamic QPI during a CT-26 cell division by using our DCMI system. First, the experimental parameters are set as the same as Section 2.3, and a closed laboratory with the temperature

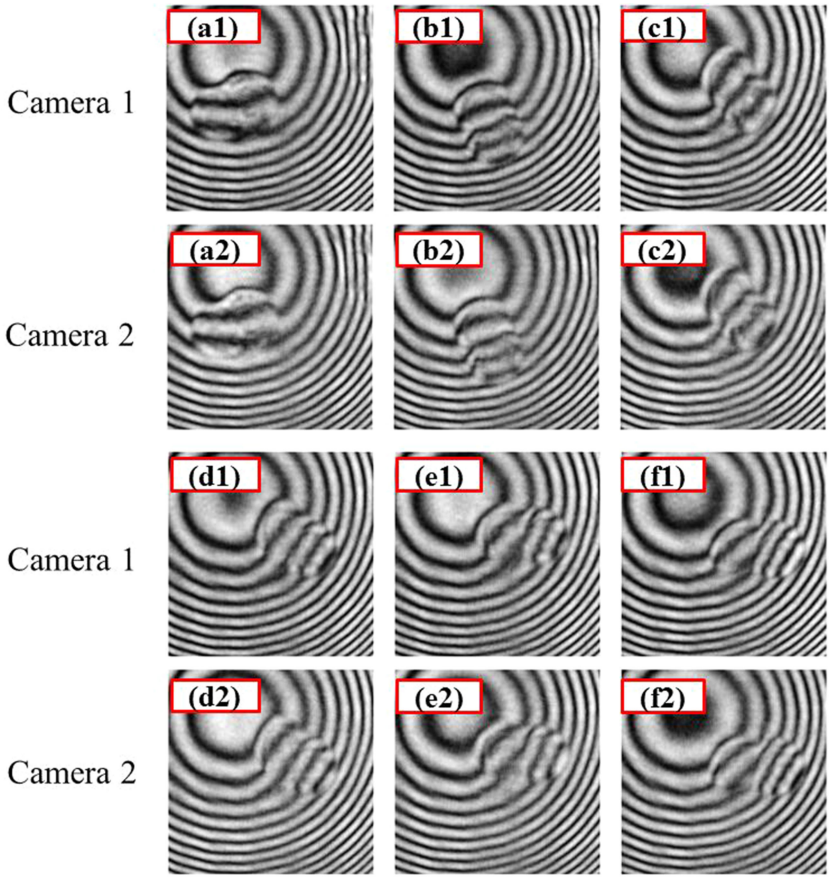

Fig. 4. Six paired-interferograms during a CT-26 cell division captured by the DCMI system, in which the size of interferogram is 400 $\times$ 400 pixels.

of 35°C and humidity at 50% is utilized to maintain the activity of living CT-26 cells. Second, a sequence of paired interferograms are captured with the speed of 3-frame/minute during CT-26 cell division, in which CT-26 cells are cultured in the chamber cover glass with the thickness of 0.5 mm. After CT-26 cells are attached to chamber cover glass, we will capture a sequence of paired interferograms by using DCMI system. As described in Section 2.2, to achieve actual cell phase, we first need to capture a pair of interferograms of culture dish and medium without CT-26 cell to remove background, and then record a sequence of paired interferograms during CT-26 cell division. Fig. 4 shows six paired-interferograms during a CT-26 cell division. Note that the captured area of six paired-interferograms is unchanged.

4. Results and Discussion

Two-step phase demodulation algorithm is utilized to calculate dynamicphase, and then the topographic information of measured living cell can be determined. Fig. 5 shows the dynamic topographic variation during a CT-26 cell division. For clarity, we also supply a Video File I (supplementary material) to visualize topographic variation during a CT-26 cell division, in which the division time of a CT-26 mother cell to two daughter cells is about 680 min.

Using Eqs. (15) and (16), we can achieve the quantitative variation of surface area and volume during a CT-26 cell division, as shown in Figs. 6(a) and (b). Interestingly, it is found that the total surface area and volume fluctuates before and after a mother cell division into two daughter cells.

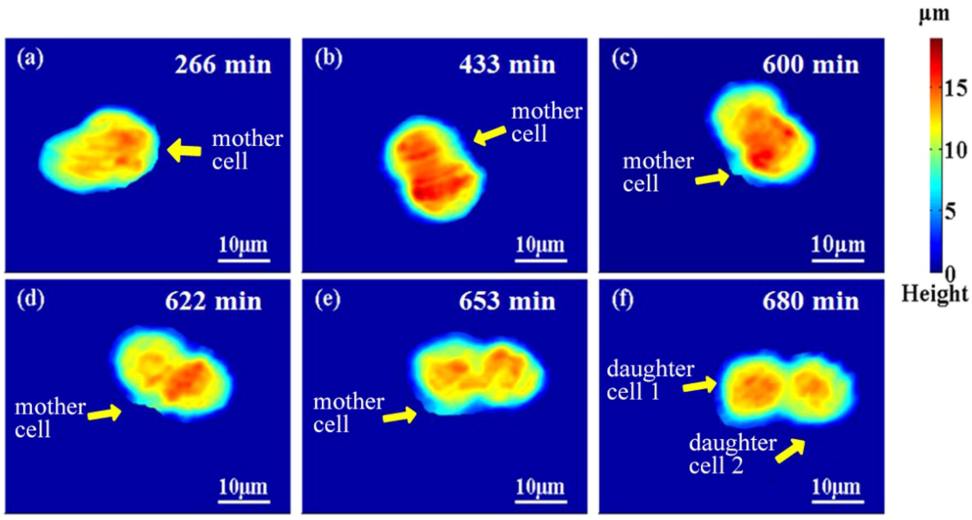

Fig. 5. Topographic variation during a CT-26cell division, in which the division time of a CT-26 mother cell to two daughter cells is about 680 min.

TABLE 1
Average Surface, Volume, and SVR of Cells Before and After the CT-26 Cell is Divided Into Two Daughter Cells

	Cell	Cell 1	Cell 2
S（um^2）	1191.6	673.5	518.1
V（um^3）	3671.1	2057.7	1613.4
SVR	0.327	0.327	0.321

After the mother cell division into two daughter cells, their surface area and volume are different, indicating that the achieved material amount of two daughter cells from mother cell are different.

Also, we can achieve the dynamic variation of the surface to volume ratio (SVR) during a CT-26 cell division into two daughter cells, shown in Fig. 6(c), in which SVR is an important parameter to represent the cellular vitality or exchange ability with the external material (culture medium) [42], [43]. Specially for our study, the parameter SVR, which represents the cell roundness, reveals the active transport of lipid droplet [44], larger SVR value indicates the flat cell with low lipid droplet transport and small SVR value indicates round cell with high lipid droplet transport rate. As we can see from Fig. 6(c), fluctuations are always existing and period fluctuations were observed from 620minutes to 645 minutes, this may suggest that steroid synthesis (steroidogenesis) [45], [46] during CT-26 cell division is not smooth and continuous. From the proposed QPI technology of DCMI system, it is found that the cell surface and volume dynamic measurement have an accuracy of sub-um2 and um3 respectively. As shown in the Table 1, although both the surface and volume of daughter cell differ greatly with mother cell, the SVR remains the same level to each other, indicating that the state of daughter cell is the same with the mother cell and the daughter cells is successfully survived after division.

As shown above, we achieved the dynamic QPI during cell division and the related parameters with high accuracy, high resolution, high stable and real-time performance. Indeed, by adjusting the polarization components of DCMI system, the phase shift between thepaired-interferograms was fixed to $\pi/2$,the synchrony mechanism and simultaneous capturing of these paired-interferograms will avoid the external noise such as vibrations and air turbulencewhich usually appeared in

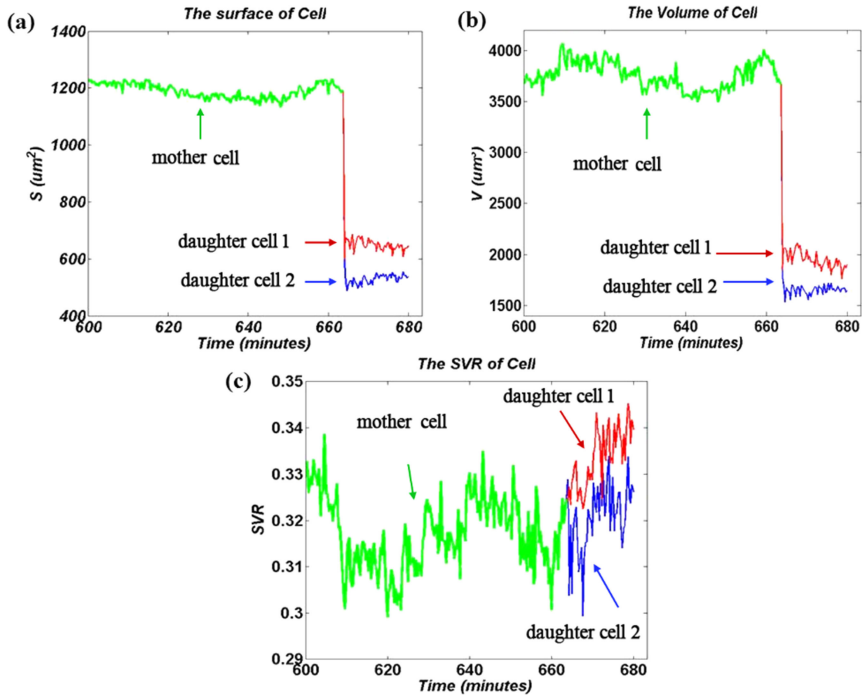

Fig. 6. Topographic information variation during a CT-26 cell division (a) the surface area variation of a CT-26 cell with time; (b) the volume variation of a CT-26 cell with time; (c) SVR variation of a CT-26 cell with time, in which the green and blue lines represent the data for mother cell and daughter cell, respectively.

the conventional methods. At the meanwhile, such fixed phase shift interferograms has advantage in phase retrieval by using less computing time and minimizing influence of interferograms inconsistence.

5. Conclusion

In this study, the QPI during cell division is implemented by our homemade DCMI system. First, by capturing a pair of interferograms with the phase shift of $\pi/2$ with the DCMI system and two-step phase demodulation algorithm, we can achieve the QPI of a livingcell, and calculate the cellular surface area, volume and the ratio of surface area to volume (RSV) and their variations. Subsequently, by capturing a sequence of paired-interferograms during cell division, we achieve dynamic QPI during cell division. It is found that before a mother cell division into two daughter cells, the total surface area and volume remain unchanged; after the mother cell division into two daughter cells, their surface area and volume are different, indicating that the achieved material amount of two daughter cells from mother cell are different. Specially, the detail SVR calculation shows that the cell roundness fluctuates mightrevealthe non-sustainability of steroid synthesis during cell division. In addition, in the last period of cell division, the SVR of daughter cell is close to that of mother cell, indicating that the state of daughter cell is the same with the mother cell and the division is successful. Both the reliability and stability of proposed DCMI method are verified. In addition to maintaining the advantages of optical interferometry, the proposed DCMI method is very suitable for QPI of dynamic process due to its rapid speed of phase retrieval. Importantly, this DCMI system will supply a powerful tool for QPI during cell division, differentiation, apoptosis and other studying dynamic processes in living cells.

References

[1] J. Reed, J. J. Troke, J. Schmit, S. Han, M. A. Teitell, and J. K. Gimzewski, "Live cell interferometry reveals cellular dynamism during force propagation," *Acs Nano*, vol. 2, p. 841, 2008.
[2] R. Kafri, J. Levy, M. B. Ginzberg, S. Oh, G. Lahav, and M. W. Kirschner, "Dynamics extracted from fixed cells reveal feedback linking cell growth to cell cycle," *Nature*, vol. 494, pp. 480–483, 2013.
[3] M. C. Drummond *et al.*, "Live-cell imaging of actin dynamics reveals mechanisms of stereocilia length regulation in the inner ear," *Nature Commun.*, vol. 6, p. 6873, 2015.
[4] Y. Gao *et al.*, "Loss of ERα induces amoeboid-like migration of breast cancer cells by downregulating vinculin," *Nature Commun.*, vol. 8, p. 14483, 2017.
[5] S. Kamlund, D. Strand, B. Janicke, K. Alm, and S. Oredsson, "Influence of salinomycin treatment on division and movement of individual cancer cells cultured in normoxia or hypoxia evaluated with time-lapse digital holographic microscopy," *Cell Cycle*, vol. 16, pp. 2128–2138, 2017.
[6] H. Majeed, C. Okoro, A. Kajdacsy-Balla, T. K. Jr, and G. Popescu, "Quantifying collagen fiber orientation in breast cancer using quantitative phase imaging," *J. Biomed. Opt.*, vol. 22, p. 46004, 2017.
[7] D. Huang *et al.*, "High speed live cell interferometry: A new method for rapidly quantifying tumor drug resistance and heterogeneity," *Analytical Chemistry*, vol. 5, pp. 3299–3306, 2018.
[8] S. Yongjin *et al.*, "Size homeostasis in adherent cells studied by synthetic phase microscopy," *Proc. Nat. Acad. Sciences United States Amer.*, vol. 110, pp. 16687–16692, 2013.
[9] G. David *et al.*, "Generation of trisomies in cancer cells by multipolar mitosis and incomplete cytokinesis," *Proc. Nat. Acad. Sciences United States Amer.*, vol. 107, pp. 20489–20493, 2010.
[10] A. Mölder, M. Sebesta, M. Gustafsson, L. Gisselson, A. G. Wingren, and K. Alm, "Non-invasive, label-free cell counting and quantitative analysis of adherent cells using digital holography," *J Microsc*, vol. 232, pp. 240–247, 2010.
[11] Y. Kim, H. Shim, K. Kim, H. J. Park, S. Jang, and Y. K. Park, "Profiling individual human red blood cells using common-path diffraction optical tomography," *Sci Rep*, vol. 4, p. 6659, 2014.
[12] W. Choi *et al.*, "Tomographic phase microscopy," *Nature Methods*, vol. 4, pp. 717–719, 2007.
[13] W. Jiang, "Hartmann-Shack wavefront sensing and wavefront control algorithm," *Adaptive Opt. Opticsal Structures*, vol. 1271, 1990.
[14] B. C. Platt and S. RV, "History and principles of Shack-Hartmann wavefront sensing," *J. Refractive Surgery (Thorofare, N.J.: 1995)*, vol. 17, pp. S573–7, 2001.
[15] F. Roddier, "Wavefront sensing and the irradiance transport equation," *Appl.Opt.*, vol. 29, pp. 1402–1403, 1990.
[16] J. Trujillo-Sevilla, J. M. Rodriguez-Ramos, L. F. Rodriguez-Ramos, and B. Javidi, "Tomographic microscopy using a plenoptic sensor," in *Inf. Opt.*, 2013.
[17] H. Li, C. Guo, and S. Jia, "High-resolution light-field microscopy," in *Frontiers Opt.*, pp. FW6D–3, 2017.
[18] C. Wu, J. Ko, and C. C. Davis, "Determining the phase and amplitude distortion of a wavefront using a plenoptic sensor," *J. Opt. Soc. Amer. A*, vol. 32, p. 964, 2015.
[19] E. Pauwels, A. Beck, Y. C. Eldar, and S. Sabach, "On fienup methods for sparse phase retrieval," *IEEE Trans. Signal Process.*, vol. 66, no. 4, pp. 982–991, 2018.
[20] J. R. Fienup, "Phase retrieval algorithms: A comparison," *Appl. Opt.*, vol. 21, pp. 2758–69, 1982.
[21] C. L. Curl *et al.*, "Single cell volume measurement by quantitative phase microscopy (QPM): A case study of erythrocyte morphology," *Cellular Physiol. Biochemistry*, vol. 17, pp. 193–200, 2006.
[22] A. Anand, V. Chhaniwal, and B. Javidi, "Quantitative cell imaging using single beam phase retrieval method," *J. Biomed. Opt.*, vol. 16, p. 060503, 2011.
[23] G. P. Frenklach I and N T. Shaked, "Off-axis interferometric phase microscopy with tripled imaging area," *Opt. Lett.*, vol. 39, pp. 1525–1528, 2014.
[24] C. R. Burch and J. P. P. Stock, "Phase-contrast microscopy," *Brit. Med. J.*, vol. 2, pp. 272–272, 1950.
[25] H. B, B. M, and Z. X, "Super-resolution fluorescence microscopy," *Annu. Rev. Biochemistry*, vol. 78, p. 993, 2009.
[26] L. Pastorek, T. Venit, and P. Hozák, "Holography microscopy as an artifact-free alternative to phase-contrast," *Histochemie*, vol. 149, pp. 179–186, 2018.
[27] T. Ikeda, G. Popescu, R. R. Dasari, and M. S. Feld, "Hilbert phase microscopy for investigating fast dynamics in transparent systems," *Opt. Lett.*, vol. 30, p. 1165, 2005.
[28] C. Fang-Yen *et al.*, "Imaging voltage-dependent cell motions with heterodyne Mach-Zehnder phase microscopy," *Opt. Lett.*, vol. 32, pp. 1572–1574, 2007.
[29] B. Kemper, A. Vollmer, C. E. Rommel, J. Schnekenburger, and B. G. Von, "Simplified approach for quantitative digital holographic phase contrast imaging of living cells," *J. Biomed. Opt.*, vol. 16, p. 026014, 2011.
[30] A. Safrani and I. Abdulhalim, "Real-time phase shift interference microscopy," *Opt. Lett.*, vol. 39, pp. 5220–5223, 2014.
[31] D. Bettenworth, A. Bokemeyer, C. Poremba, N. S. Ding, and B. Kemper, "Quantitative phase microscopy for evaluation of intestinal inflammation and wound healing utilizing label-free biophysical markers," *Histology Histopathology*, vol. 33, pp. 417–432, 2018.
[32] G. Popescu, K. Badizadegan, R. R. Dasari, and M. S. Feld, "Errata: Observation of dynamic subdomains in red blood cells," *J. Biomed. Opt.*, vol. 11, p. 040503, 2006.
[33] N. Pavillon *et al.*, "Early cell death detection with digital holographic microscopy," *Plos One*, vol. 7, p. e30912, 2012.
[34] Y. Xiao, M. Cross, C. Liu, D. C. Clark, D. T. Haynie, and M. K. Kim, "Measurement of the traction force of biological cells by digital holography," *Biomed. Opt. Express*, vol. 3, pp. 153–159, 2012.
[35] O. Y. Kwon, "Multichannel phase-shifted interferometer," *Opt. Lett.*, vol. 9, pp. 59–61, 1984.
[36] M. N. J. Brock, "Methods and apparatus for splitting, imaging, and measuring wavefronts in interferometry," 2006.
[37] K. Creath and J. Schmit, "Interferometry XII: Techniques and analysis," in *Proc. SPIE - Int. Soc. Opt. Eng.*, vol. 4777, pp. 159–183, 2008.

[38] D. C. Ghiglia and L. A. Romero, “Robust two-dimensional weighted and unweighted phase unwrapping that uses fast transforms and iterative methods,” *J. Opt. Soc. Am. A*, vol. 11, pp. 107–117, 1994.
[39] A. J. Levine, G. Popescu, L. Millet, M. U. Gillette, R. Wang, and Z. Wang, “Dispersion-relation phase spectroscopy of intracellular transport,” *Opt. Express*, vol. 19, pp. 20571–20579, 2011.
[40] T. Kim, R. Zhou, L. L. Goddard, and G. Popescu, “Solving inverse scattering problems in biological samples by quantitative phase imaging,” *Laser Photon. Reviews*, vol. 10, pp. 13–39, 2016.
[41] K. Itoh, "Analysis of the phase unwrapping algorithm,” *Appl. Opt.*, vol. 21, p. 2470, 1982.
[42] W. M. Lewis, “Surface/volume ratio: Implications for phytoplankton morphology,” *Science*, vol. 192, pp. 885–887, 1976.
[43] S. L. Nielsen and K. S. Jensen, “Allometric settling of maximal photosynthetic growth rate to surface/volume ratio,” *Limnology Oceanogr.*, vol. 35, pp. 177–181, 1990.
[44] X. Nan, E. O. Potma, and X. S. Xie, “Nonperturbative chemical imaging of organelle transport in living cells with coherent anti-stokes Raman scattering microscopy,” *Biophysical J.*, vol. 91, pp. 728–735, 2006.
[45] G. Betz and P. F. Hall, “Steroidogenesis in adrenal tumor cells: Influence of cell shape,” *Endocrinology*, vol. 120, p. 2547, 1987.
[46] N. Gallo-Payet and M. D. Payet, “Mechanism of action of ACTH: Beyond cAMP,” *Microsc Res Tech*, vol. 61, pp. 275–287, 2010.